

# Steady and Unsteady Two-dimensional Turbulent Flow over E193 Airfoil

Soha Yusuf\* and Habeeb Idris †  
662011092 662056401

In this project, we perform CFD analysis for steady and unsteady turbulent flow over E193 airfoil with chord length 0.3m. Turbulent flow analysis is performed for Reynolds number  $Re_c = 1.01 \times 10^6$  for fixed and dynamic mesh. 6 meshes are created to study the effect of first layer thickness and number of mesh layers on surface y plus and how adjusting these variables could impact mesh and result accuracy. Similarly, 5 meshes were used for the plunging airfoil case to find trade-off between the limitation imposed by computational cost which strongly depends on the size of mesh. Optimum meshes M01, M05 and M06 are identified for  $Re_c = 1.01$  million at 0°, 10° and 5° angles of attack respectively. In this investigation, 0 degree angle of attack is used for all dynamic mesh CFD simulations and three different angles of attack are used for steady turbulent flow over asymmetric airfoil.

## I. Problem Description

### A. Geometry

The geometry of interest for this CFD analysis is asymmetric Eppler airfoil, E193. The coordinates were gotten from Airfoil Tools [1]. It is an asymmetric airfoil that generates lift at zero angle of attack. We created the geometry for quasi-3D modeling, with an airfoil chord length of  $c = 0.3\text{m}$  and span  $0.2c = 0.3 = 0.06\text{m}$  (20% of chord length), using Solidworks. The airfoil is enclosed in a circular boundary of diameter  $100c$  (30m) as shown in Fig 1.

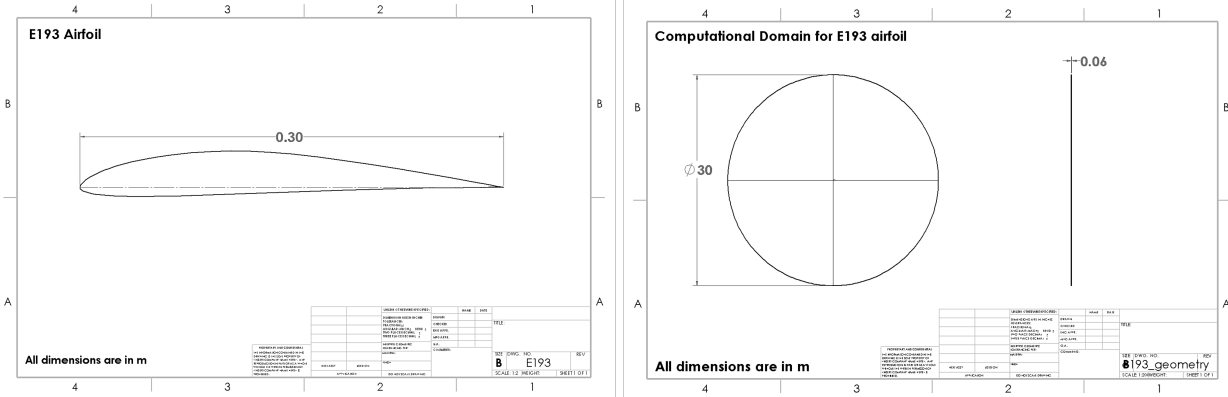


**Fig. 1 (Left)** E193 airfoil with chord length  $c = 0.3\text{m}$  **(Right)** Computational domain with diameter of  $100c = 30\text{m}$ .

### B. Equations

The first aspect of the CFD analysis is steady flow over the Eppler airfoil which is set up to be incompressible. Governing equations for steady incompressible flow is governed by Navier-Stokes equations:

$$\rho \left( \frac{\partial u_j}{\partial t} + u_i \frac{\partial u_j}{\partial x_i} \right) = \rho g_j - \frac{\partial p}{\partial x_j} + \mu \frac{\partial^2 u_j}{\partial x_i^2} + (\mu + \lambda) \frac{\partial}{\partial x_j} \frac{\partial u_m}{\partial x_m} \quad (1)$$

\*Rensselaer Polytechnic Institute

†Rensselaer Polytechnic Institute

The second aspect of this analysis is transient flow for plunging airfoil. The vertical oscillation (plunging) of the airfoil in y-direction is given by:

$$d_y(t) = A_{osc} \sin\left(\frac{2\pi t}{T_{osc}}\right) = A_{osc} \sin(2\pi f_{osc} t) = A_{osc} \sin(\omega_{osc} t) \quad (2)$$

where,  $A_{osc}$  is the amplitude of the oscillation,  $T_{osc}$  is the time period of oscillation and  $f_{osc}$  is the frequency of the oscillation.

### C. Material

For this analysis, we use air as the fluid with Mach number  $Ma = 0.204$  and Reynolds number  $Re = 1.18 \times 10^6$ . Table 1 shows the material properties for air.

**Table 1 Material Properties of Fluid (Air)**

Property	Symbol	Fluid (Air)
Density ( $\text{kg/m}^3$ )	$\rho$	1.225
Kinematic Viscosity ( $\text{m}^2/\text{s}$ )	$\nu$	$1.781 \times 10^{-5}$

### D. Physical conditions

The analysis is performed for subsonic, incompressible flows such that  $Ma < 0.3$ . For air, Mach number and Reynolds number are calculated as follows:

$$Ma = \frac{\text{velocity of fluid}}{\text{speed of sound}} \quad (3)$$

$$Re_c = \frac{U_c}{\nu} \quad (4)$$

The numerical values used for CFD analysis is summarized in table 2 below.

**Table 2 Flow conditions**

Condition	Symbol	Steady Flow	Unsteady Flow
Free Stream Velocity (m/s)	$U_\infty$	70	60
Reynolds Number	$Re_c$	$1.18 \times 10^6$	$1.01 \times 10^6$
Mach Number	$Ma$	0.204	0.1749

[Individual contribution: Habeeb (50%), Soha (50%)]

## II. Problem Setup

Prior to running simulations, we set up the problem for the CFD analysis. This includes defining the time marching option, modeling type, and the boundary conditions. The setup are grouped into two; steady state setup with fixed mesh and unsteady setup with moving mesh.

### A. Boundary conditions for steady flow over fixed mesh

The problem is set up as steady, time independent, for the first track where different angles of attack are simulated for. For this setting, the fluid flow is simulated for condition where the flow properties such as velocity doesn't change with time.

Boundary conditions are constraints defined at the boundaries of computational domains and determines how solutions are obtained at those boundaries (see Figure 2). For this problem, we applied three boundary conditions:

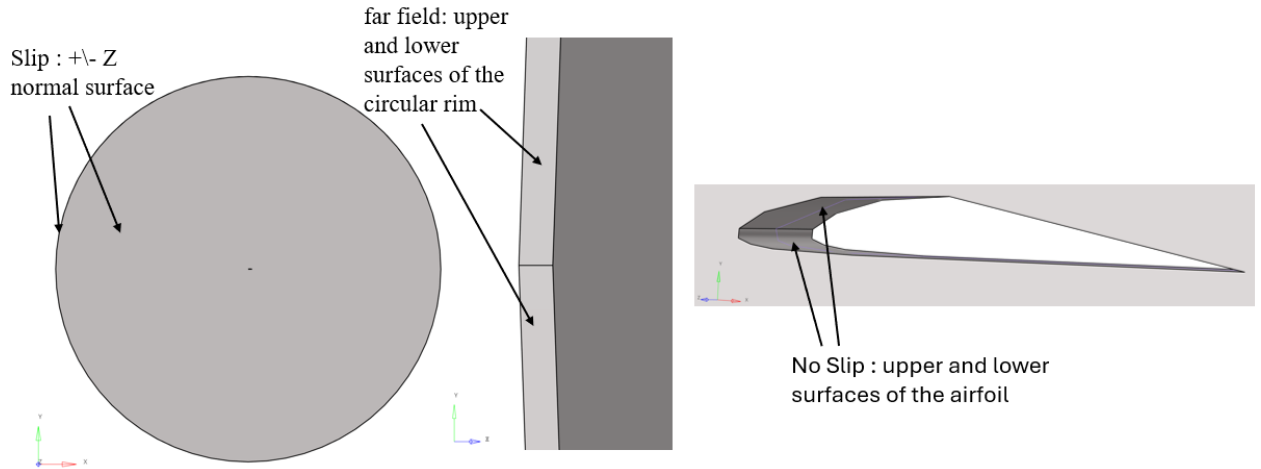


**Fig. 2 Boundary conditions: slip , far-field and no slip (left to right)**

- No slip: this boundary condition is specified on the surface of airfoil where the velocity of the fluid is zero. The fluid sticks to the boundary due to viscosity of the fluid and this leads to the formation of boundary layers where viscous effects are dominant. No slip boundary condition is represented mathematically as:

$$u = 0 \quad (5)$$

where,  $u$  is the velocity of the fluid. In the software, we set the near-wall treatment to "wall resolved" because it is a boundary condition in a computational domain that's used to define the fluid velocity at the wall surface. In addition to this, the "wall velocity type" was set to "zero". Since we are using viscous fluids, this setting ensures that the fluid adheres to the surface [2].

- Far field: free stream velocity  $U_\infty$  is constant far away from the airfoil. The freestream/far field velocity is set to  $U_\infty = 70\text{m/s}$
- Slip: this boundary condition is used at the surface where there is no change in the tangential velocity and the normal velocity is zero [2], i.e.

$$u_{normal} = 0 \quad (6)$$

and

$$\frac{\partial u}{\partial x_i} = 0 \quad (7)$$

where  $x_i$  is the tangential direction of that surface. We applied this boundary condition on the  $+/- Z$  normal surface because we want the free stream velocity to be uniform up till where we have impact of the airfoil presence in the domain.

These boundary condition details are summarized in Table 3

The cases were ran for different angles of attack and the velocity setup in the far field boundary condition is detailed in Table 4

**Table 3 Boundary Conditions**

Boundary Condition	Location	Additional Information
No Slip	Upper and lower wall of airfoil	Set “Near-wall treatment” to ‘Wall Resolved’ “Roughness height” to 0 Set “Wall velocity type” to ‘Zero’
Far Field	Upper and lower surfaces of the circular rim	Set velocity as 70 m/s
Slip	+/- Z normal surfaces	

**Table 4 Far field velocities for different angles of attack**

Flow Speed (m/s)	Angle of Attack(deg)	x Velocity(m/s)	y Velocity(m/s)
70	0	70.00	0
70	5	69.73	6.10
70	10	68.94	12.16

### B. Boundary conditions for unsteady flow over plunging airfoil

The second track of the simulation is set up for transient analysis where User-Defined Function (UDF) is used to define the unsteady, plunging airfoil problem, along the y-axis, as expressed earlier in Equation (2) with the details in Table 5 below.

The boundary condition is the same as that of the first track with steady flow setup but with the no slip boundary condition set up with wall velocity type "match mesh velocity" and far field free stream velocity  $U_\infty = 60\text{m/s}$ .

### C. Turbulence

Turbulence is a fluid mechanics terms that implies the irregular and chaotic flow of fluids which can involve the presence of swirls, eddies, and vortex. Unlike laminar flow with smooth flow, turbulence flow is not smooth and occurs at high Reynolds number. Since we are working with high Reynolds number of order  $10^6$ , we set up the problem for turbulence modeling. From the available turbulence modeling options on Altair Hyperworks CFD, Spalart-Allmaras was selected because it was originally designed for aerodynamic applications and works well for modeling turbulent flows around airfoils and wings. Both the steady and the unsteady cases are set up for turbulence CFD simulation.

[Individual contribution: Habeeb (50%), Soha (50%)]

**Table 5** Plunging airfoil oscillation parameters

Parameter	symbol	Formula	Value
Chord length	c	-	0.3 m
Free-stream velocity	$U$	-	70 m/s
Constant	$c1$	-	0.4
Constant	$c2$	-	3
Amplitude	$A_{osc}$	$(c1)c$	0.12
Time period	$T_{flow}$	$D/U$	0.005
Time period of oscillation	$T_{osc}$	$2(c2)T_{flow}$	0.03
Frequency of oscillation	$\omega_{osc}$	$2\pi/T_{osc}$	209.44
Time step	$dt$	$T_{flow}/16$	0.0003125
Simulation time	$T_{sim}$	$5T_{osc}$	0.15
No. of steps	N	$T_{sim}/dt$	480
Simulation steps per frame	$N_s$	$N/40$	12

### III. Simulation Details

#### A. Numerical Scheme

We kept AcuSolve default settings.

#### B. Mesh Setup For Steady Flow

Sequel to setting up the problem, more than 60% of the time was spent generating and refining the mesh to have good results. For most of the cases, we added Edge mesh, Edge Layer mesh, box refinement zone, surface mesh, extrusion, and volume mesh.

##### 1. Edge Mesh

We created mesh for the two edge surfaces of the airfoil on the +Z normal face and set the average element size, for the final mesh, to  $c/128 = 2.3475 \times 10^{-3}$ . This is to ensure that we are able to get good solution at the airfoil surface.

##### 2. Edge Layer Mesh

We add edge layer mesh in order to be able to capture the effect of velocity gradient and viscosity near the airfoil surface. It helps to have improved resolution of boundary layer and enhance the accuracy of flow predictions. This feature add meshing layers that grows outward from the two airfoil curved edges (the upper and lower airfoil curves) on the +Z normal face it's applied on.

##### 3. Rectangular Refinement Zone

We added a rectangular refinement zone to the +Z normal face, around the airfoil to further refine the mesh around the airfoil. The refinement was limited to be from just before the airfoil leading and some regions behind the trailing edge to effectively capture the action-regions, for instance, we have the stagnation point at the airfoil leading edge, velocity and viscous effects at the upper and lower airfoil curves, and the wake, flow separation, eddies and vortex at the region after/behind the trailing edge. Thus applying the rectangular refinement helps to get more accurate flow prediction at these regions.

#### 4. Surface Mesh

With surface mesh, we create mesh on the entire domain surface on the +Z normal face. With the refinements and edge layer mesh specified close to the airfoil surface, the mesh around this region are very fine. Conversely, mesh farther away from the airfoil are coarse because there little to no action going on in these far-field areas. For this reason, we set the mesh size to be "Maximum Size" and maximum element to be  $c = 0.3$  for the surface mesh.

#### 5. Mesh Extrusion

For our quasi-3D mesh, after setting the aforementioned mesh controls, we extrude the mesh generated on the +Z normal face to go through the span. Since this span have been defined to be  $0.2c$ , we set element size along extrusion to be  $0.2c$  (i.e.  $0.2 \times 0.3 = 0.06$ ) and the element type is set to be quads. This implies that there is only one mesh element along the extrusion depth.

#### 6. Volume mesh

We use the volume mesh to generate the mesh for the whole volume with all the earlier defined mesh settings/controls. We also set the mesh size here to be "Maximum Size" and maximum element to be  $c = 0.3$ .

The general mesh setting can be summarized as follows:

##### 1) Edge

- Select the two edge curves of the airfoil on the +Z normal face
- Average element size:  $c/128 = 2.34375 \times 10^{-3}$

##### 2) Edge layer

- select the two edge curves of the airfoil on the +Z normal face
- First layer thickness:  $c/10^5 = 3 \times 10^{-6}$
- Total number of layers: 30
- Growth method: Constant
- Growth rate: 1.25
- Termination policy: 'Truncate'
- Enable surface mesh modification

##### 3) Rectangular refinement zone

- Length  $x = 2.2c = 2.2 \times 0.3 = 0.66$
- Height  $y = 0.6c = 0.3 \times 0.3 = 0.018$
- Depth  $z = 0.3c = 0.3 \times 0.36 = 0.09$
- Average element size:  $c/128 = 2.34375 \times 10^{-3}$

##### 4) Surface

- Select the domain surface on +Z normal face for the surface mesh
- Mesh size: 'Maximum Size'
- Maximum element size:  $c = 0.3$

##### 5) Extrusion

- Element size along extrusion:  $c/5 = 0.3/5 = 0.06$

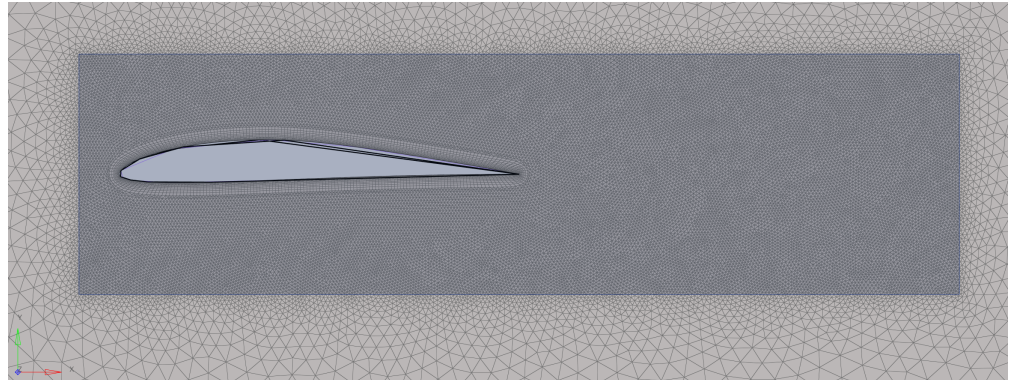
##### 6) Volume

- Mesh size: 'Maximum Size'
- Maximum element size to  $c = 0.3$

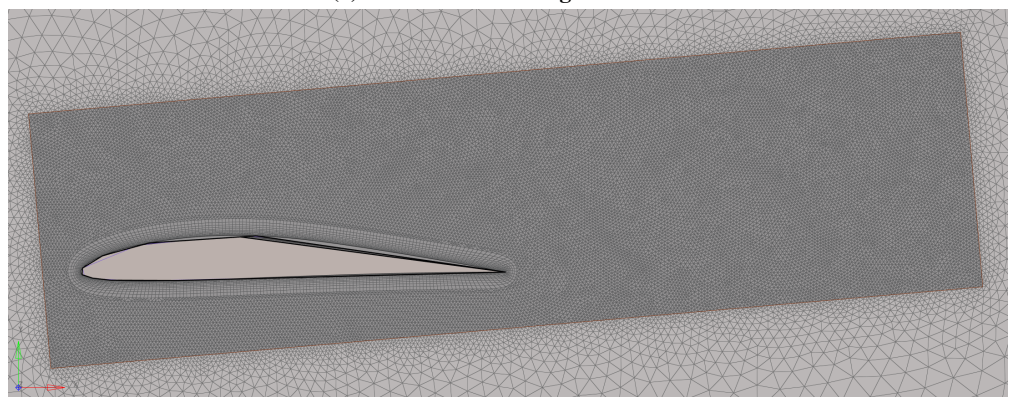
The result of these settings is as shown in Figure 3a. In order to effectively capture the action areas at downstream and around the airfoil at  $5^\circ$  and  $10^\circ$  angles of attack, the rectangular refinements are rotated in the +Z direction (counterclockwise) by these angles ( $5^\circ$  and  $10^\circ$ ) such that the top and bottom surfaces of the rectangular box refinement zones are tangential/parallel to the freestream flow directions as shown in Fig 3b and 3c.

## C. Mesh Setup For the Unsteady Flow

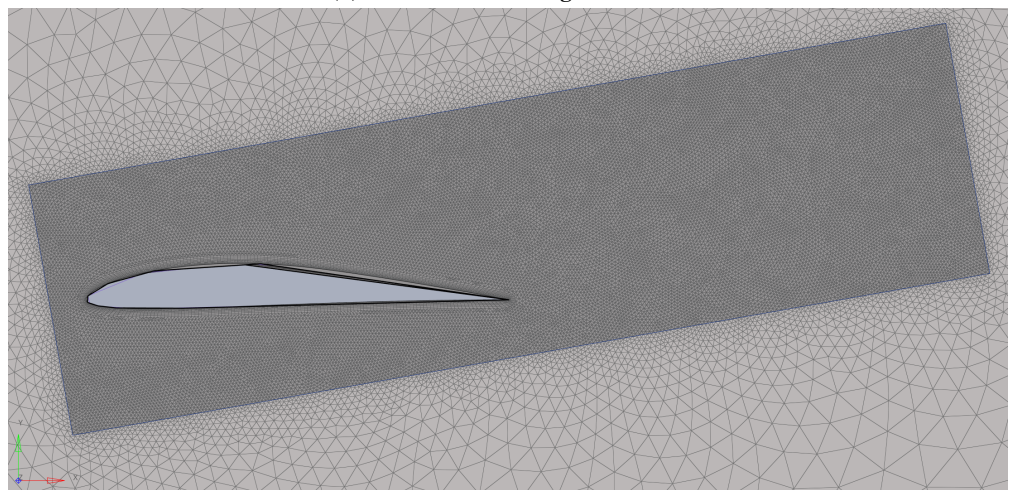
The mesh setting for the unsteady flow is similar to the steady flow mesh setting but with more coarse element sizes as detailed in Table 7.



(a) Mesh M01 at  $0^\circ$  angle of attack



(b) Mesh M06 at  $5^\circ$  angle of attack



(c) Mesh M05 at  $10^\circ$  angle of attack

**Fig. 3 Steady flow mesh for different angles of attack**

#### D. Plunging Airfoil Motion Setting

Running the simulation for plunging requires a bit more settings beyond the steady CFD simulation. The motion settings can be summarized as follows:

1) Translation

- Select "Translation under Motion"
- Select "Surfaces"
- Select the two curved surfaces of the airfoil
- Select "Vector"
- Select +y direction for movement
- Select Sinusoidal from the dropdown and click on "/" to get the options
- Amplitude = 0.12
- Frequency = 209.44
- Repeat Translation for the two far field curved boundary surfaces to a 'Constant' motion of 0

2) Settings

- Mesh Motion: Mesh Motion = Arbitrary

3) Planar Slip

- Select the 'Planar Slip' tool
- Select the +/- Z circular surfaces individually in two separate instances for the two surfaces

The flow physics setup is defined based on Equation 2 and Table 5 and could be summarized in the following steps as:

- Go to the Flow ribbon and select Physics in Setup
- Select incompressible under 'Single phase flow'
- Set Time marching to 'Transient'
- Time step size: 0.0003125 (dt)
- Final time: 0.15 ( $T_{sim}$ )
- Turbulence model: Spalart-Allmaras

**[Individual contribution: Habeeb (50%), Soha (50%)]**

#### IV. Additional Details

This section entails mesh details, effect of first layer thickness and number of layers on mesh quality for two different problems - steady fixed mesh and unsteady dynamic mesh - at Reynolds number  $Re_c = 1.01 \times 10^6$ . We created 6 fixed meshes for steady turbulent flow over E193 airfoil summarized in Table 6. Similarly, we created 5 dynamic meshes for unsteady turbulent flow over E193 airfoil summarized in Table 7. This resulted from trying different mesh settings and adjusting to get good mesh, desirable surface y plus, and get mesh convergence.

**Table 6 Mesh details for 6 fixed meshes at different angles of attack for steady turbulent flow over E193 airfoil**

Mesh name	Angle of attack	$U_\infty$	Fluid	Avg element size	First layer thickness	No. of layers
M01	0°	70	Air	c/128	$c/10^5$	30
M02	0°	70	Air	c/128	$c/10^5$	35
M03	5°	70	Air	c/256	$c/10^5$	30
M04	10°	70	Air	c/128	$c/10^5$	30
M05	10°	70	Air	c/128	$c/(2.5 \times 10^5)$	35
M06	5°	70	Air	c/128	$c/(2.5 \times 10^5)$	35

**Table 7 Mesh details for 5 meshes at 0° angle of attack for unsteady turbulent flow over plunging airfoil**

Mesh name	Domain	$U_\infty$	Fluid	Re	Avg element size	First layer thickness	No. of layers
U01	Rectangle	2	Air	$6 \times 10^2$	c/32	$c/32$	10
U02	Farfield	2	Air	$6 \times 10^2$	c/16	$c/16$	5
U03	Farfield	50	Air	$1.5 \times 10^4$	c/64	$c/64$	5
U04	Farfield	60	Air	$1.01 \times 10^6$	c/32	$c/32$	10
U05	Farfield	60	Air	$1.01 \times 10^6$	c/64	$c/128$	10

**Table 8 Mesh oscillation details for 5 different meshes for flow over plunging (moving mesh) airfoil**

Mesh	Domain	Turbulence model	Ma	c1	c2	$A_{osc}$	$w_{osc}$	dt	$T_{sim}$	Num_steps
U01	Rectangle	Laminar	0.0058	0.4	3	0.12	6.981	0.009375	4.5	480
U02	Fairfield	Laminar	0.0058	0.4	3	0.12	6.981	0.009375	4.5	480
U03	Fairfield	Laminar	0.1458	0.4	3	0.12	174.5	0.000375	0.18	480
U04	Fairfield	Spalart-Allmaras	0.1749	0.4	3	0.12	209.4	0.0003125	0.15	480
U05	Fairfield	Spalart-Allmaras	0.1749	0.4	3	0.12	209.4	0.0003125	0.15	480

The mesh images for U01 - U05 are shown in the figures below.

##### A. Effect of number of layers and first layer thickness on mesh quality

Generally, increasing the number of layers and decreasing the first layer thickness for the edge layer mesh control increase the mesh quality and yield better result. However, there has to be a balance between how the first layer thickness and number of layers are adjusted, otherwise, there could be bad transition from the quadrilateral mesh elements to the triangular mesh elements. This was experienced in M04 and M05, as shown in Figure 9.

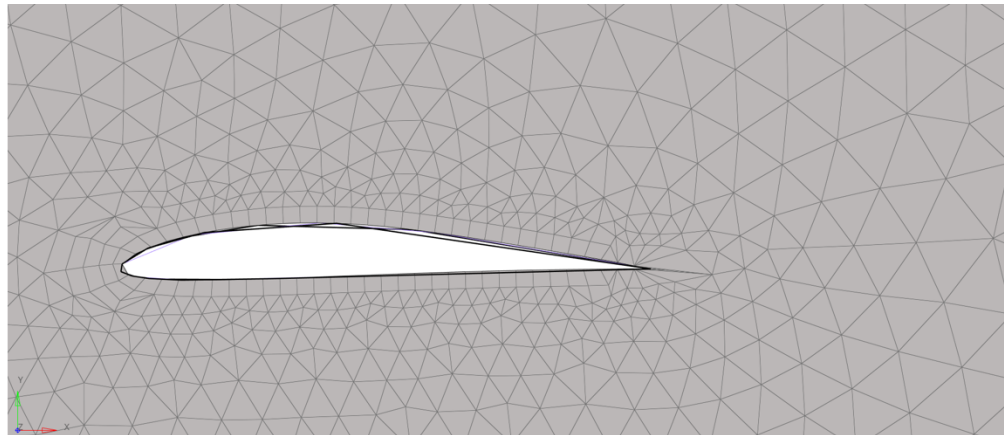


**Fig. 4** Mesh U01

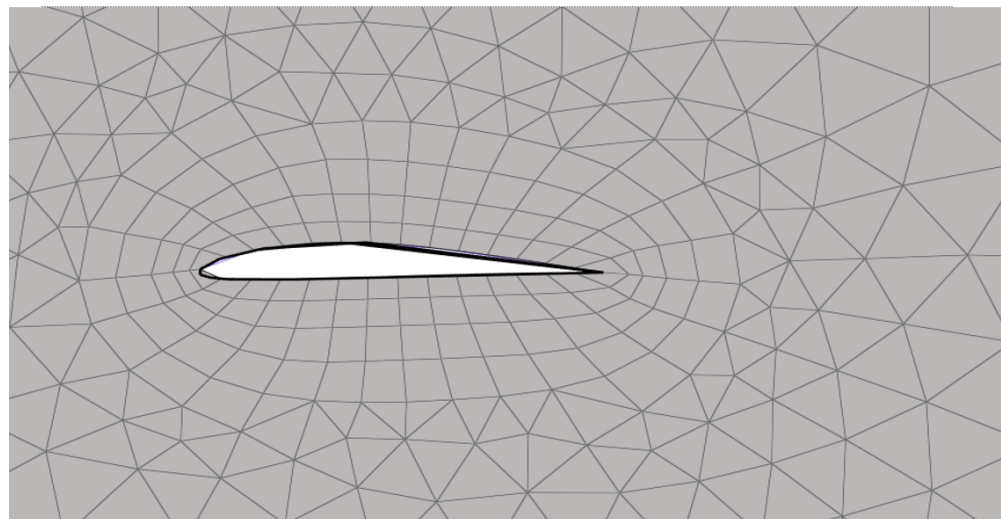


**Fig. 5** Mesh U02

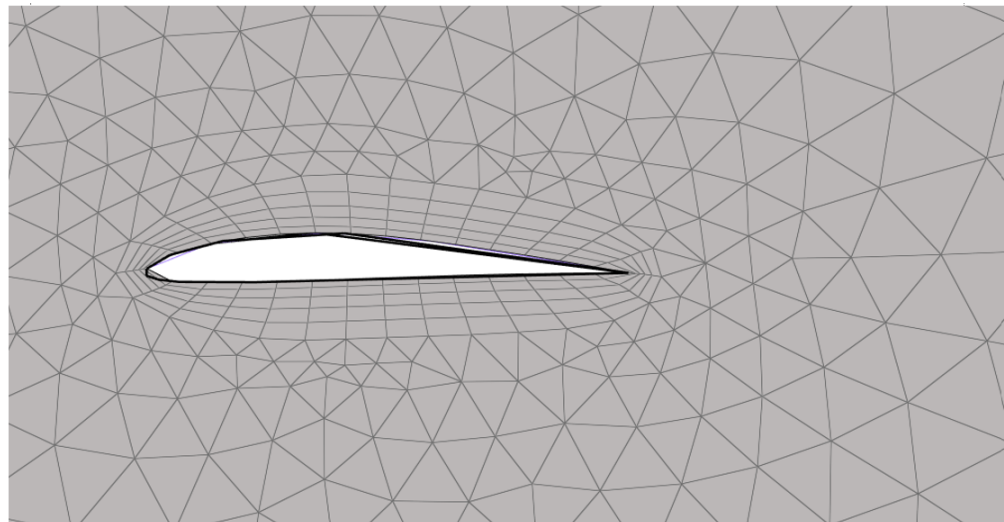


**Fig. 6** Mesh U03

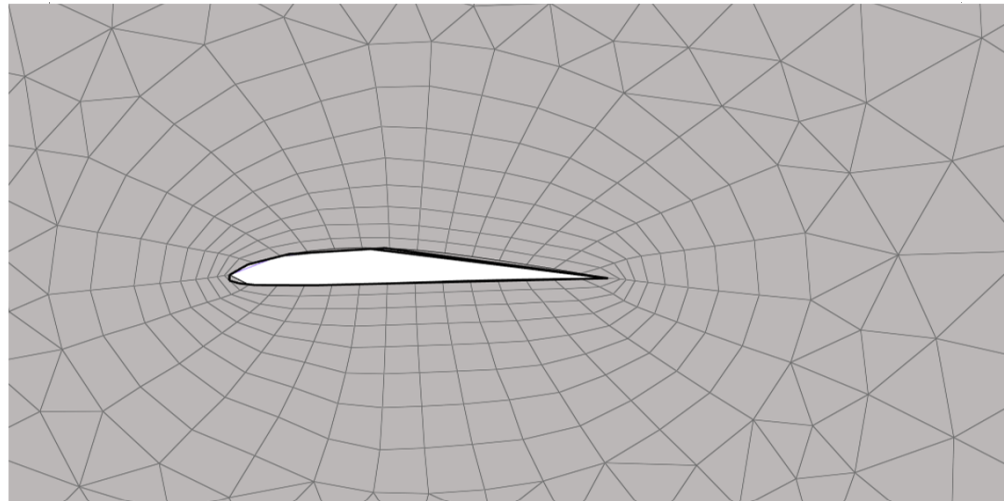


**Fig. 7** Mesh U04

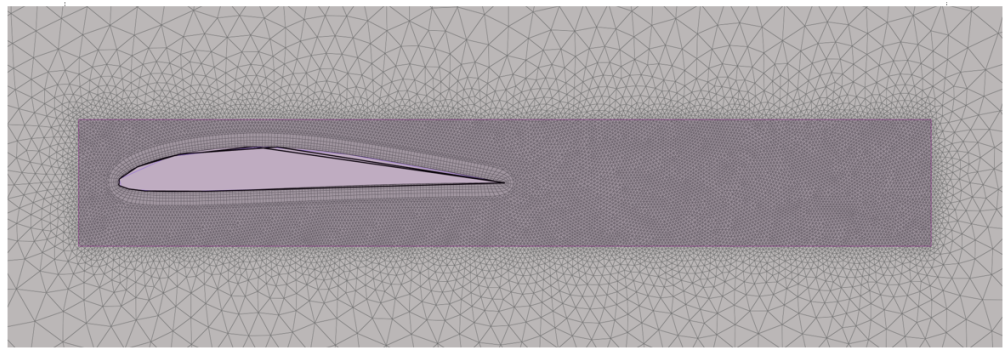


**Fig. 8** Mesh U05

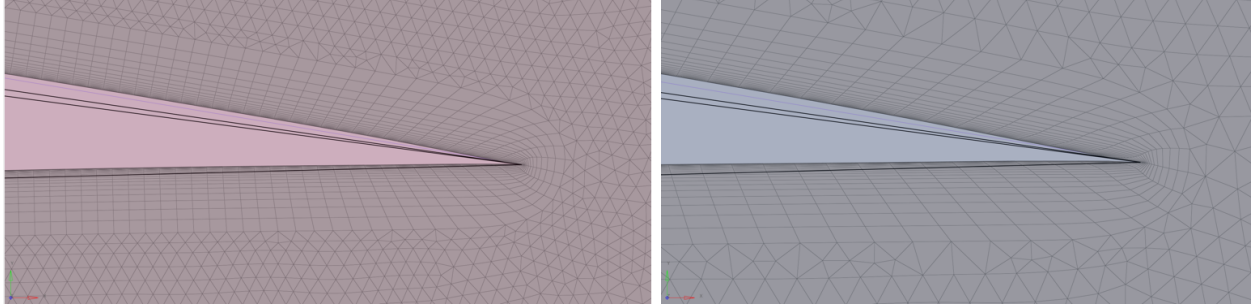


**Fig. 9** (left) Mesh M04 with first layer thickness of  $c/10^5$  produces a mesh with defects such that the transition is not smooth. (Right) Mesh M05 with first layer thickness of  $c/(2.5 \times 10^5)$  results in smoother transition from quadrilateral elements to triangular elements.

### B. Average element size

We used average element sizes of  $c/128$  and  $c/256$  which strongly increased the computational cost of simulation. This led to maintaining average element size of  $c/128$  throughout this analysis, which suffice for the desired result.

$$\frac{c}{128} = \frac{0.3}{128} = 0.00234375m \quad (8)$$

### C. Quality Report

The quality report for all the meshes created (M01 - M10) are listed in the tables below (Table 9 - 19).

**Table 9 Quality Report for M01**

Type	Count
Nodes	107616
Surface mesh elements	198934
Volume mesh elements	99118
Triangles	182636
Quadrilaterals	16298
Tetrahedral elements	0
Hexahedral elements	7800
Pyramid elements	0
Prism elements	91318

**Table 10 Quality Report for M02**

Type	Count
Nodes	94936
Surface mesh elements	170341
Volume mesh elements	84785
Triangles	150810
Quadrilaterals	19531
Tetrahedral elements	0
Hexahedral elements	9380
Pyramid elements	0
Prism elements	75405

**Table 11 Quality Report for M03**

Type	Count
Nodes	107406
Surface mesh elements	198514
Volume mesh elements	98908
Triangles	182216
Quadrilaterals	16298
Tetrahedral elements	0
Hexahedral elements	7800
Pyramid elements	0
Prism elements	91108

**Table 12 Quality Report for M04**

Type	Count
Nodes	106996
Surface mesh elements	197694
Volume mesh elements	98498
Triangles	181396
Quadrilaterals	16298
Tetrahedral elements	0
Hexahedral elements	7800
Pyramid elements	0
Prism elements	90698

**Table 13 Quality Report for M05**

Type	Count
Nodes	110442
Surface mesh elements	201986
Volume mesh elements	100644
Triangles	183088
Quadrilaterals	18898
Tetrahedral elements	0
Hexahedral elements	9100
Pyramid elements	0
Prism elements	91544

**Table 14 Quality Report for M06**

Type	Count
Nodes	109168
Surface mesh elements	199438
Volume mesh elements	99370
Triangles	180540
Quadrilaterals	18898
Tetrahedral elements	0
Hexahedral elements	9100
Pyramid elements	0
Prism elements	90270

**Table 15 Quality Report for U01**

Type	Count
Nodes	23110
Surface mesh elements	45614
Volume mesh elements	22575
Triangles	45008
Quadrilaterals	606
Tetrahedral elements	0
Hexahedral elements	71
Pyramid elements	0
Prism elements	22504

**Table 16 Quality Report for U02**

Type	Count
Nodes	40166
Surface mesh elements	79614
Volume mesh elements	39574
Triangles	178896
Quadrilaterals	718
Tetrahedral elements	0
Hexahedral elements	126
Pyramid elements	0
Prism elements	39448

**Table 17 Quality Report for U03**

Type	Count
Nodes	40374
Surface mesh elements	80002
Volume mesh elements	39768
Triangles	79256
Quadrilaterals	746
Tetrahedral elements	0
Hexahedral elements	140
Pyramid elements	0
Prism elements	39628

**Table 18 Quality Report for U04**

Type	Count
Nodes	39880
Surface mesh elements	78816
Volume mesh elements	39175
Triangles	77872
Quadrilaterals	944
Tetrahedral elements	0
Hexahedral elements	239
Pyramid elements	0
Prism elements	38936

**Table 19 Quality Report for U05**

Type	Count
Nodes	69972
Surface mesh elements	136646
Volume mesh elements	67974
Triangles	133348
Quadrilaterals	3298
Tetrahedral elements	0
Hexahedral elements	1300
Pyramid elements	0
Prism elements	66674

## V. Results

### A. Steady turbulent flow over E193 airfoil (fixed mesh)

#### 1. Surface Y Plus

Surface  $y$  plus decreases as the first layer thickness in the mesh is decreased. The observations from the results are given below:

- As the first layer thickness decreases, the surface  $y^+$  values decrease exponentially, indicating a finer resolution of the near-wall region.
- At a given Reynolds number, different meshes exhibit distinct surface  $y^+$  values for the same first layer thickness, suggesting variations in grid resolution and accuracy.
- For both Reynolds numbers, the surface  $y^+$  values tend to approach lower values as the first layer thickness decreases, signifying better representation of the near-wall flow features.

Table below shows surface  $y$  plus for 6 different meshes. Note that best surface  $y$  plus values are obtained for meshes M01, M05 and M06 at three different angles of attack.

**Table 20**  $C_L$  and  $C_D$  at  $Re_c = 1.01 \times 10^6$  for steady turbulent flow over E193 airfoil

Mesh	Angle of attack	surface $y^+$	D	L	$C_D$	$C_L$
M01	0°	0.911	0.57753	19.484	0.01069	0.36066
M02	0°	1.280	0.57038	19.444	0.01056	0.35992
M03	5°	1.060	3.40280	47.875	0.06299	0.88620
M04	10°	1.270	9.56810	65.689	0.17711	1.21596
M05	10°	0.262	9.60260	65.712	0.17775	1.21638
M06	5°	0.428	3.40390	48.044	0.06301	0.88933

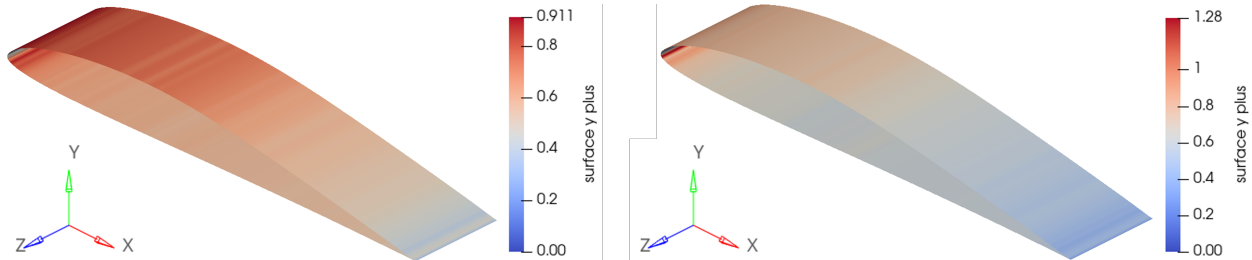


**Fig. 10** Surface  $y$  plus at  $Re_c = 1.01 \times 10^6$  for Mesh M01 (left) and Mesh M02 (right) at 0° angle of attack.

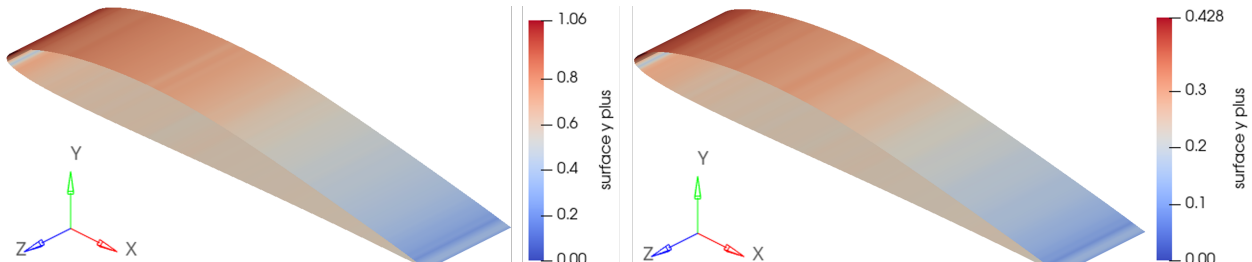


**Fig. 11** Surface  $y$  plus at  $Re_c = 1.01 \times 10^6$  for Mesh M03 (left) and Mesh M06 (right) at 5° angle of attack.

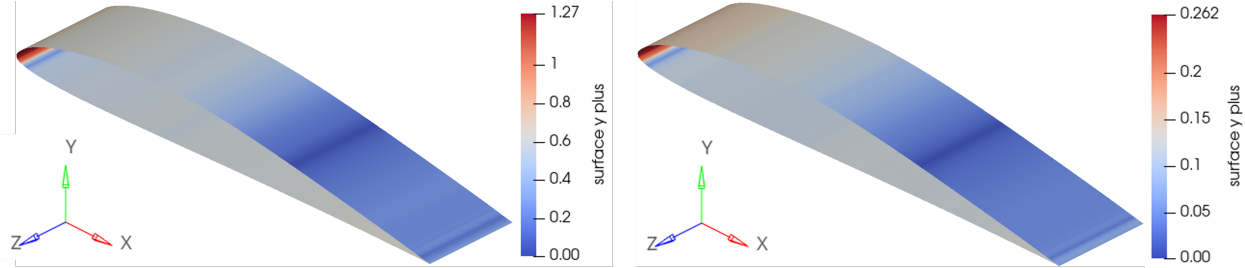


**Fig. 12** Surface  $y$  plus at  $Re_c = 1.01 \times 10^6$  for Mesh M04 (left) and Mesh M05 (right) at  $10^\circ$  angle of attack.

## 2. Lift and Drag Coefficients

The lift and drag forces corresponds to the x and y traction forces from the CFD software. It's known, a-priori, that as the angle of attack increases, lift and drag coefficients increase. This is shown posteriori with the CFD result as summarized in Table 20. The  $C_L$  value generally increases up to a certain critical point beyond which further increase in the angle of attack leads to decrease in lift coefficient. This phenomenon is called stalling but not experienced in this CFD analysis.

## 3. Velocity

Velocity plots at  $Re_c = 1.01 \times 10^6$  for  $0^\circ$ ,  $5^\circ$  and  $10^\circ$  angles of attack are shown in figures 13, 14 and 15 respectively. The blue areas around the leading edge and the trailing edge represents the regions of zero/minimal velocity. The blue region at the leading edge is the stagnation point where the fluid velocity is zero which follows the knowledge of aerodynamics, at zero angle of attack. Similarly, the region at the trailing edge represents the location where fluid from the upper and lower airfoil surfaces join, at low/zero velocity. Just behind the trailing edge is the flow separation region. This flow separation region isn't wide because the airfoil is at zero degree angle of attack, and for this reason, trailing edge eddies and vortex would be minimal, unlike turbulent flow over an airfoil at some angle of attack.

The maximum velocity could be noticed in red color at the upper and lower surfaces of the airfoil because the flow accelerates from the leading edge (at zero velocity) to the maximum thickness point on the airfoil surface, where the velocity is maximum, then decelerates towards the trailing edge.

Observations for velocity plots for turbulent flow over the E193 airfoil at  $0^\circ$ ,  $5^\circ$ , and  $10^\circ$  angles of attack with a Reynolds number of 1.01 million:

### 1) At $0^\circ$ angle of attack

Near the leading edge, boundary layer forms as the flow separates from the airfoil surface. The flow follows the contour of the airfoil, accelerating over the upper surface and reaching maximum velocity near the trailing edge. Along the lower surface of airfoil, the flow velocity is lower compared to the upper surface due to the pressure difference across the airfoil. We observe separation zone in the wake region of airfoil where velocity is minimum due to boundary layer separation.

### 2) At $5^\circ$ angle of attack

The flow separation point moves closer to the leading edge compared to  $0^\circ$  angle of attack. The upper surface flow accelerates further and experiences stronger turbulence due to increased flow interaction with the airfoil surface. The lower surface flow exhibits more significant separation, especially towards the trailing edge.

### 3) At $10^\circ$ angle of attack

Flow separation point moves further towards the leading edge. Increased separation on both the upper and lower surfaces, indicating a more significant loss in lift and potential increase in drag. Stronger vortices or turbulent structures might be visible in the wake region, indicating increased aerodynamic instability.

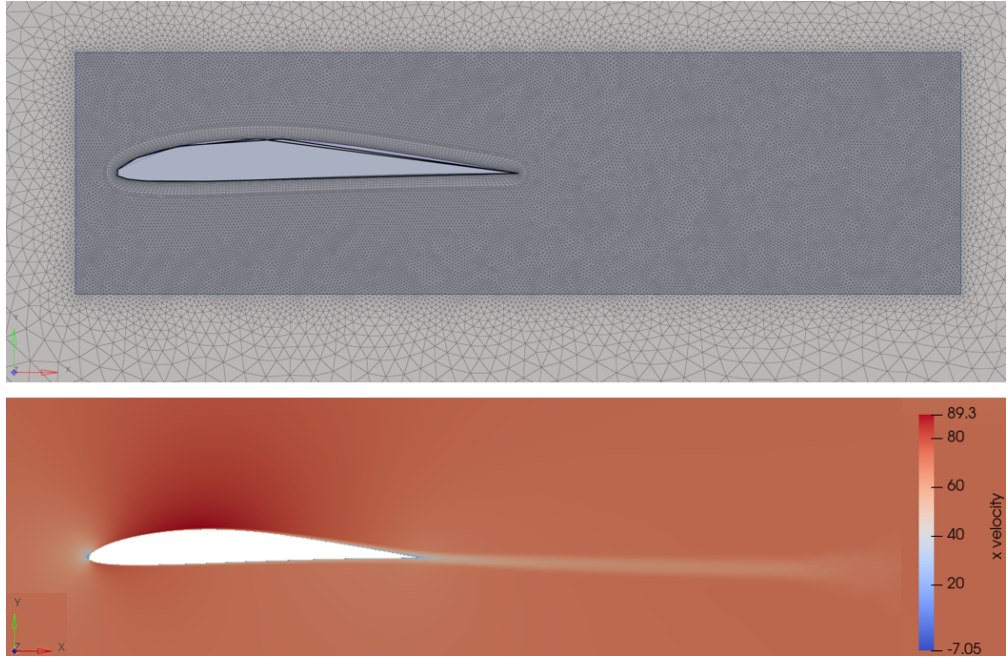


**Fig. 13** (Top) Mesh M01 with average element size of  $c/128$  and total 99118 number of elements (Bottom) Velocity contour plot for  $\text{Re}_c = 1.01 \times 10^6$  for the corresponding mesh. Blue region near the airfoil represents boundary layer where viscous effects are dominant. Fluid velocity away from the airfoil reached free stream velocity of  $U_\infty = 70\text{m/s}$ .

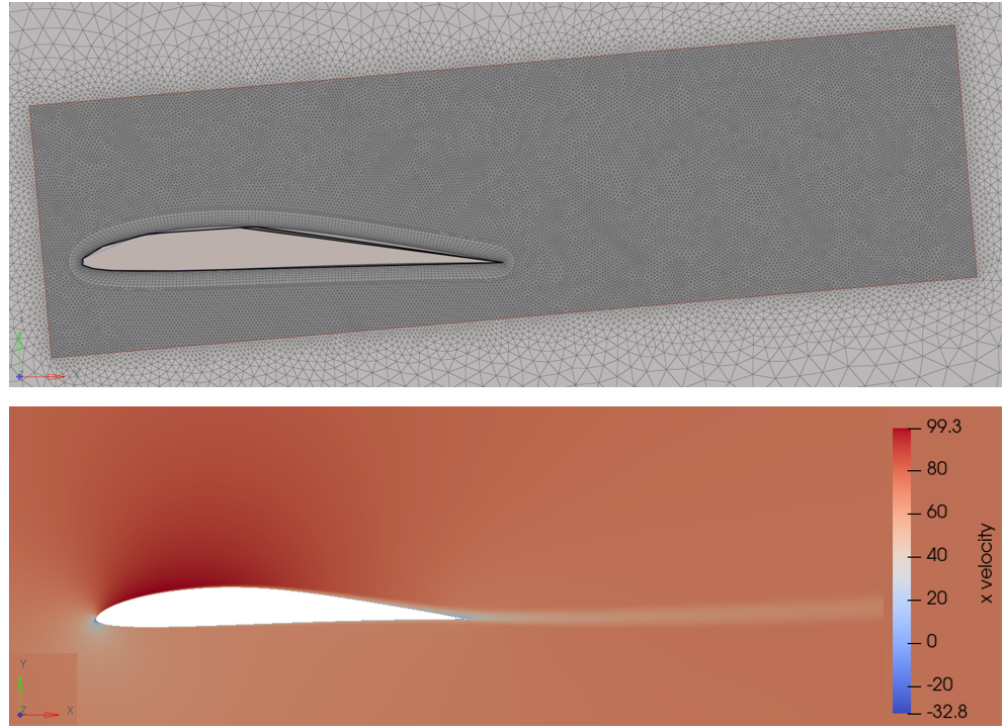


**Fig. 14** (Top) Mesh M06 at  $5^\circ$  angle of attack with average element size of  $c/128$  and total 99370 number of elements (Bottom) Velocity contour plot for  $\text{Re}_c = 1.01 \times 10^6$  for the corresponding mesh. Blue region near the airfoil represents boundary layer where viscous effects are dominant. Fluid velocity away from the airfoil reached free stream velocity of  $U_\infty = 70\text{m/s}$ .

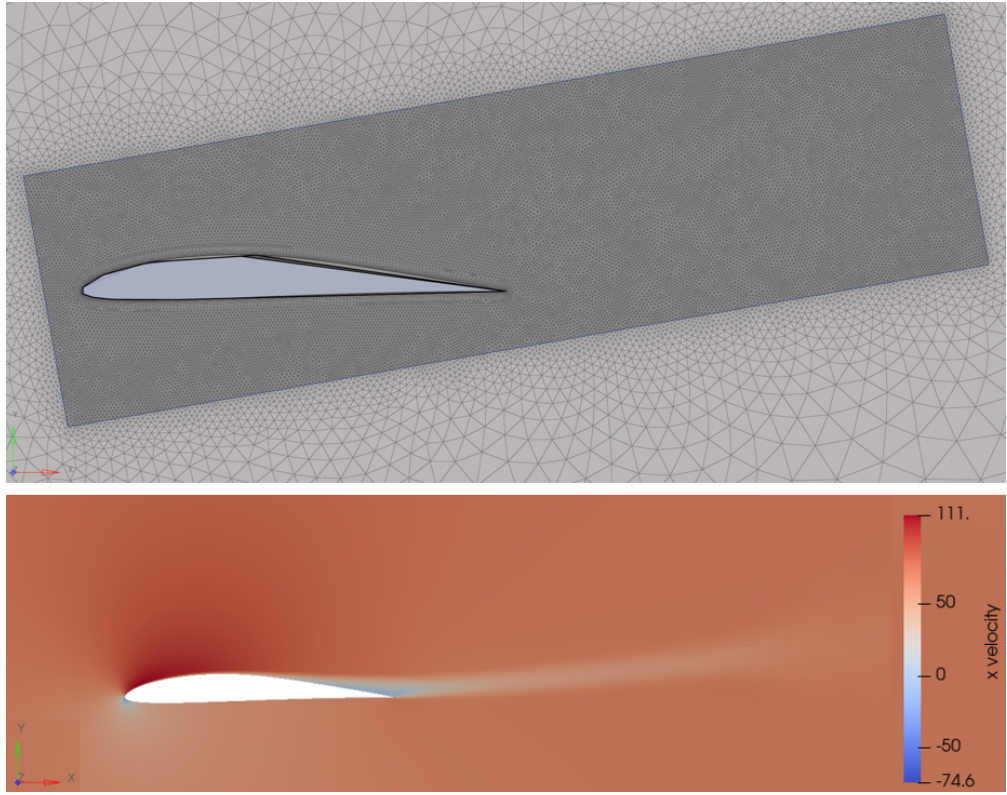


**Fig. 15** (Top) Mesh M05 at  $10^\circ$  angle of attack with average element size of  $c/128$  and total 100644 number of elements (Bottom) Velocity contour plot for  $Re_c = 1.01 \times 10^6$  for the corresponding mesh. Blue region near the airfoil represents boundary layer where viscous effects are dominant. Fluid velocity away from the airfoil reached free stream velocity of  $U_\infty = 70\text{m/s}$ .

#### 4. Traction

The traction forces in the x and y directions represents the lift and drag, respectively, on the airfoil surface. The lift and drag coefficients are calculated with

$$C_L = \frac{L}{\frac{1}{2}\rho b c U_\infty^2} \quad (9)$$

and

$$C_D = \frac{D}{\frac{1}{2}\rho b c U_\infty^2} \quad (10)$$

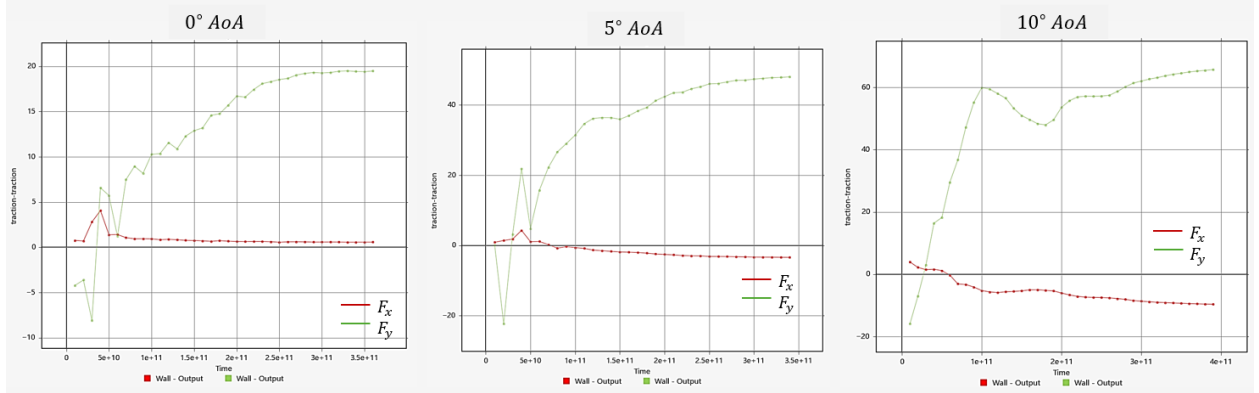


**Fig. 16** Lift and drag force plot for  $\text{Re}_c = 1.01 \times 10^6$  for  $0^\circ$  (left),  $5^\circ$  (middle) and  $10^\circ$  (right) angles of attack.

## B. Unsteady turbulent flow over plunging E193 airfoil (dynamic mesh)

### 1. Surface Y Plus

Surface  $y$  plus is greater than 1 for plunging airfoil due to insufficient number of mesh elements - 39175 elements for U04 and 67974 elements for U05. Mesh refinement is computationally expensive, which limited the level of refinement we used for this analysis. Figures 17 and 17 shown oscillating airfoil and corresponding surface  $y$  plus at 6 different time frames.

Surface  $y$  plus decreases as the first layer thickness in the mesh is decreased. As the first layer thickness decreases, the maximum surface  $y^+$  values decrease exponentially, indicating a finer resolution of the near-wall region.

**Table 21 Surface  $y$  plus for meshes U04 and U05 for plunging airfoil at time frame 40**

Mesh	Turbulence model	surface $y^+$	Maximum y traction	Minimum y traction
U04	Spalart-Allmaras	662	71.316	-63.033
U05	Spalart-Allmaras	181	74.336	-60.022

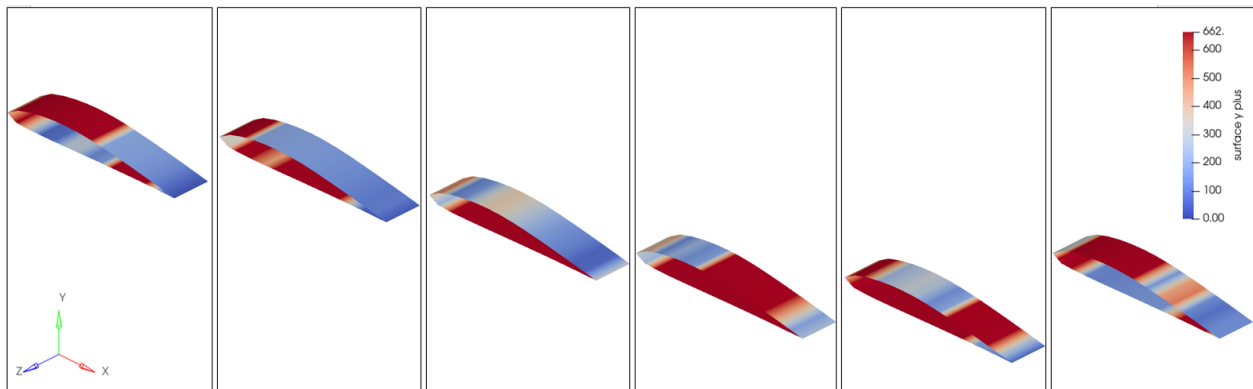


**Fig. 17 Surface  $y$  plus for mesh U04 at frames 34, 35, 36, 37, 38 and 39 (left to right), showing the oscillation of airfoil and magnitude of maximum surface  $y$  plus.**

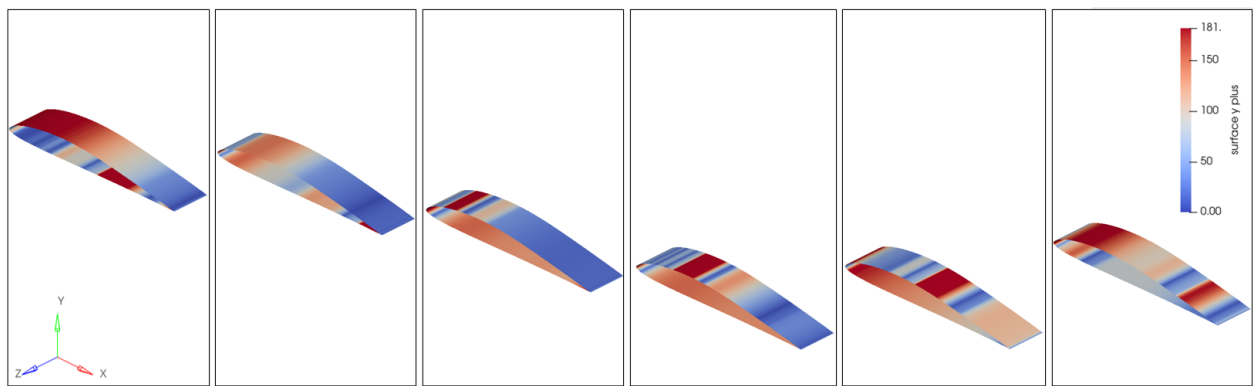


**Fig. 18 Surface  $y$  plus for mesh U05 at frames 34, 35, 36, 37, 38 and 39 (left to right), showing the oscillation of airfoil and magnitude of maximum surface  $y$  plus.**

## 2. Velocity

The velocity plots show how the flow field evolves over time. Velocity fields for plunging airfoil at  $Re= 1.01$  million is shown for different time frames in figures 19, 20 and 21.

In laminar flow over an airfoil shown in Figure 19, the inlet flow velocity uniform and matches the freestream velocity. At the leading edge, the velocity decreases slightly due to the boundary layer forming along the surface. However, there's no abrupt change in velocity at the leading edge, unlike in turbulent flow. Along the airfoil surface, the velocity decreases gradually within the boundary layer, where the fluid adheres to the airfoil surface due to viscosity. This decrease in velocity is more pronounced closer to the surface and leads to a velocity gradient within the boundary layer. The point of maximum velocity occurs slightly above the airfoil's surface, within the boundary layer. This maximum velocity corresponds to the point where the boundary layer transitions from laminar to turbulent flow, known as the transition point. In laminar flow, separation occurs more smoothly compared to turbulent flow, with the separation point farther downstream along the airfoil surface. As shown in the Figure below, vortices form in the wake region. These vortices are shed alternately from each side of the object. This phenomenon, known as vortex shedding, is pronounced in this flow due to low Reynolds number  $Re= 600$ .

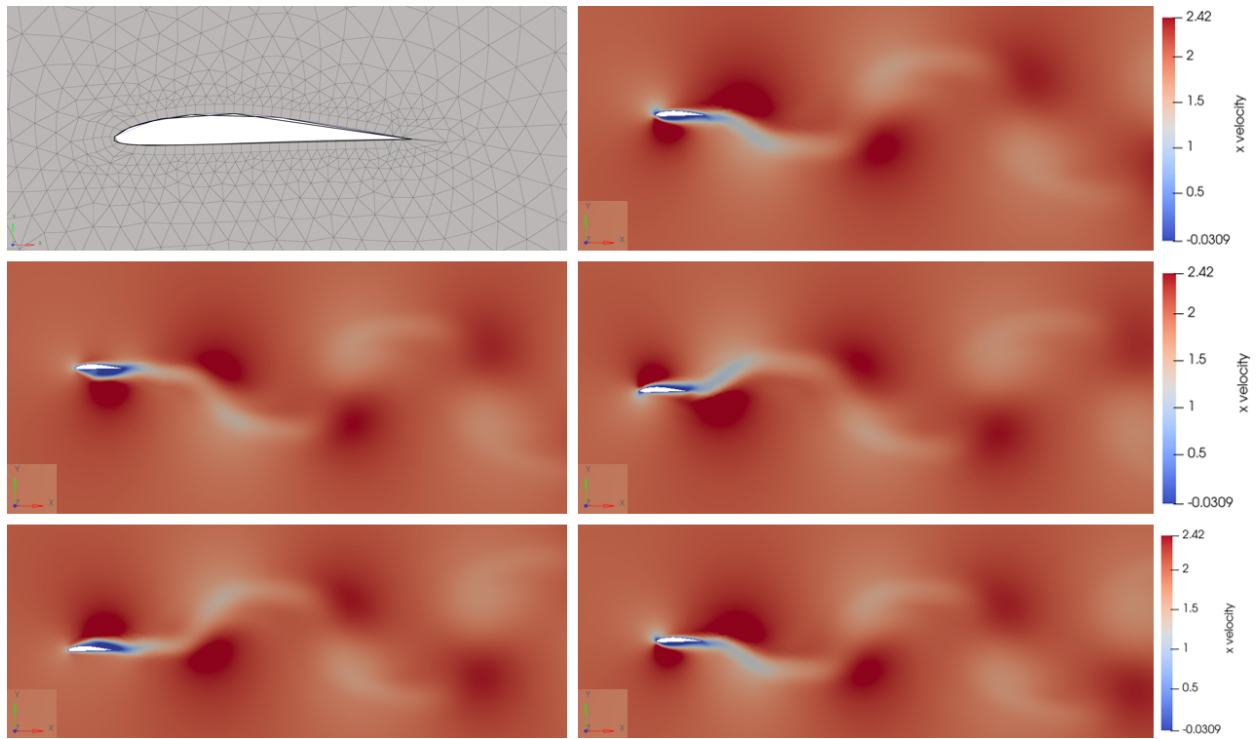


**Fig. 19 Velocity for mesh U01 with plunging airfoil at frames 36, 37, 38, 39 and 40 for  $Re=1.01$  million**

In turbulent flow over an oscillating airfoil, as shown in Figures 20 and 21, the velocity distribution is characterized by dynamic and irregular fluctuations due to the presence of turbulent eddies and vortices. Turbulent flow is unsteady and chaotic, characterized by fluctuations in velocity and pressure. When an airfoil undergoes oscillatory motion, these fluctuations become even more pronounced due to the interaction between the airfoil motion and turbulent eddies in the flow. At the beginning of the oscillation cycle, the velocity distribution around the airfoil depends on its instantaneous position and orientation. As the airfoil oscillates, the velocity distribution changes rapidly in response to the changing flow conditions. Near the leading edge, the velocity fluctuates rapidly as the flow separates and reattaches to the airfoil surface during each oscillation cycle as shown in figures below.

In the wake of the oscillating airfoil, turbulent mixing and vorticity generation lead to the formation of a complex wake structure shown by swirling eddies and vortices. These structures persist downstream of the airfoil and contribute to the overall turbulence levels in the flow.

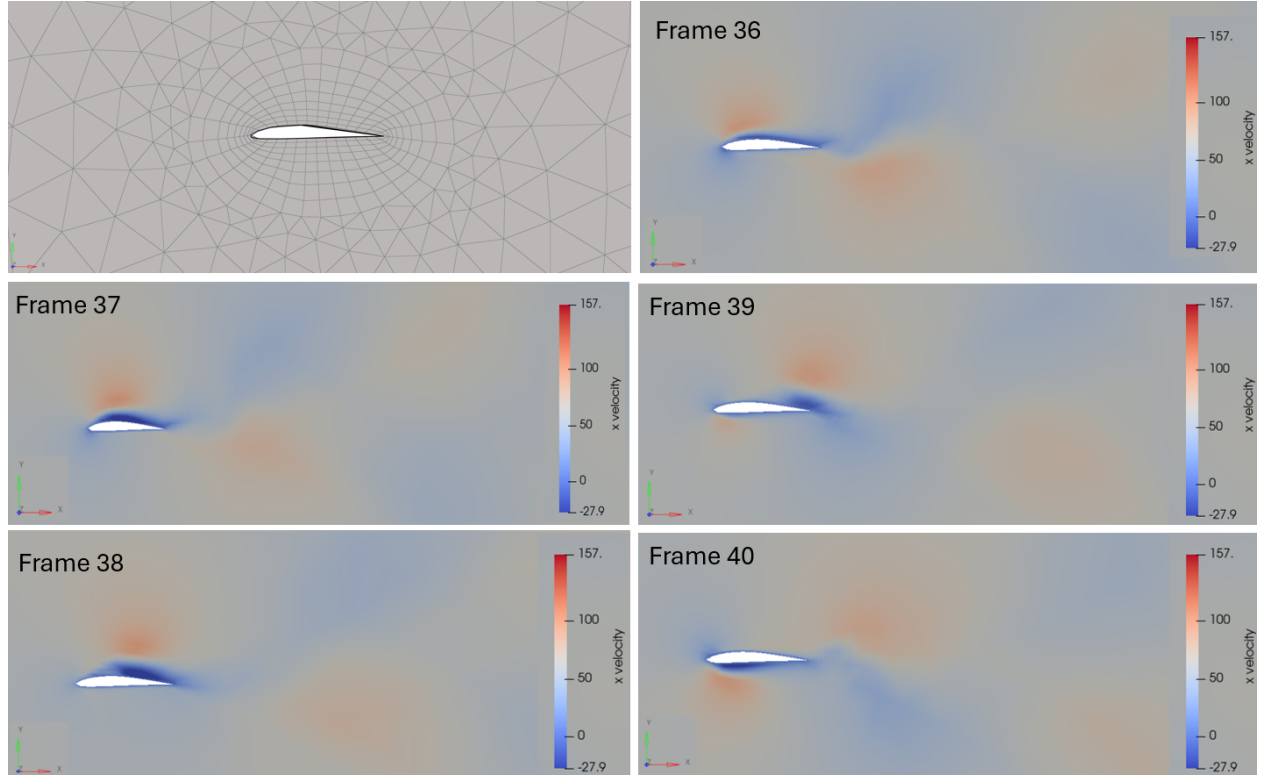


**Fig. 20 Velocity for mesh U04 with plunging airfoil at frames 37, 38, 39 and 40 for  $Re=1.01$  million**

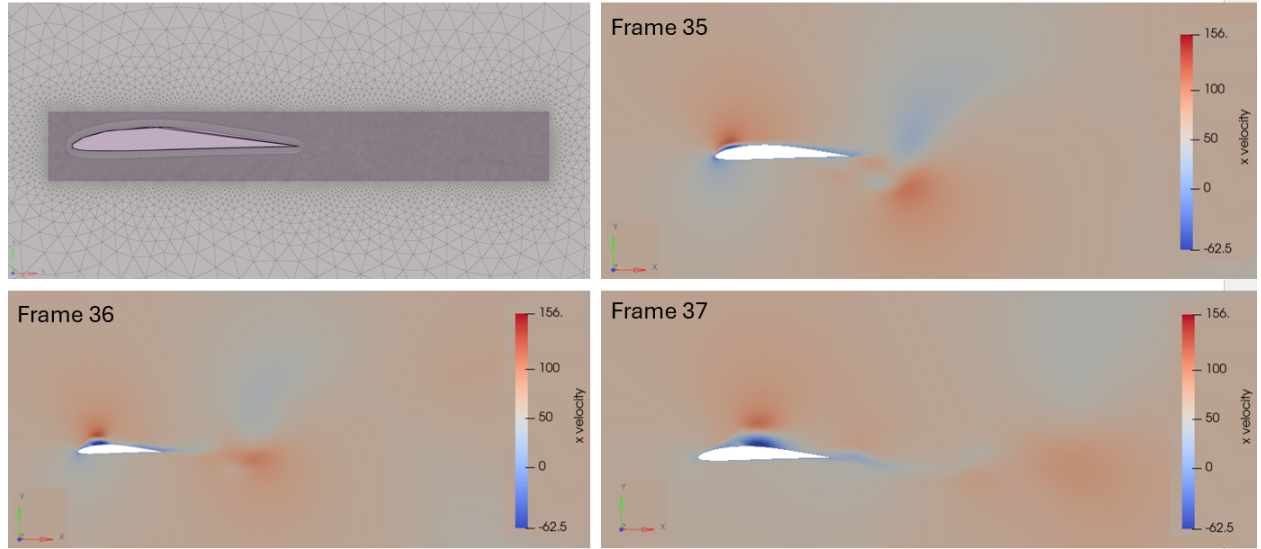


**Fig. 21 Velocity for mesh U05 with plunging airfoil at frames 37, 38, 39 and 40 for  $Re=1.01$  million**

### 3. Traction

The plots in Figure 22 show y traction force using meshes U04 and U05. The oscillating motion of airfoil in this analysis is captured in y traction at the wall as shown in figure below.

[Individual contribution: Habeeb (50%), Soha (50%)]

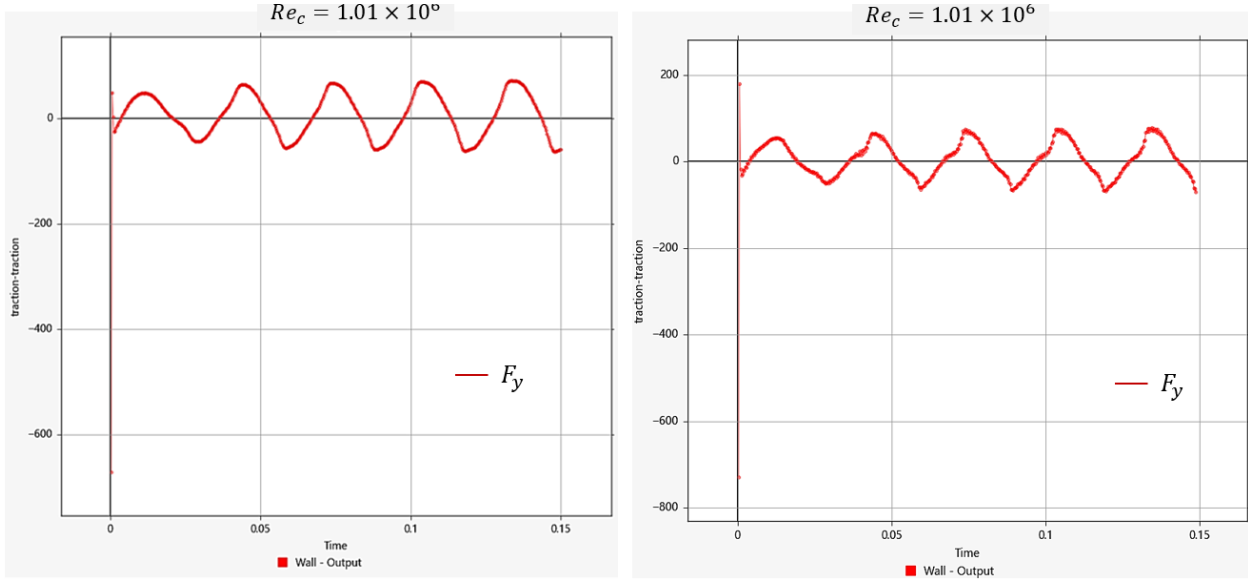


**Fig. 22 Velocity for mesh U04 (left) and U05 (right) with plunging airfoil at frames 37, 38, 39 and 40 for  $Re=1.01$  million**

## VI. Conclusion

In this project, we performed computational fluid dynamic analysis for:

- 1) steady turbulent flow over airfoil at three different ( $0^\circ$ ,  $5^\circ$  and  $10^\circ$ ) angles of attack
- 2) unsteady turbulent flow over plunging airfoil at  $0^\circ$  angle of attack

For case 1 (steady flow over fixed mesh), we observe as angle of attack increase the separation point moves towards the leading edge, lift force increases and area of wake region increase at the trailing edge of airfoil. We used 2 different meshes for each angle of attack and observed that surface  $y$  plus decreases as first layer thickness is decreased. In this investigation, we observe that surface  $y$  plus decreases as the first layer thickness is decreased, although it is noteworthy to be careful in reducing the first layer thickness and take note of the number of layers being used in order to ensure smooth transition from the layered mesh to the unlayered mesh. Too much reduction in the first layer thickness, without the appropriate growth rate and number of layers could result in short-height layered mesh which won't effectively cover boundaries around the airfoil surface i.e. the boundary layer where viscous effects are dominant.

For case 2 (unsteady flow over plunging airfoil), we observe the formation of significant eddy currents in the wake region as the airfoil oscillated. Also, increase the frequency of oscillation increases the vorticity. We used 2 different meshes U04 and U05 for turbulent flow over airfoil in farfield and mesh U01 for laminar flow over airfoil in rectangular domain.

**[Individual contribution: Habeeb (50%), Soha (50%)]**

## References

- [1] NASA, “Airfoil Tools (4-Digit NACA Airfoil Generator),” , 2024. URL <http://airfoiltools.com/airfoil/naca4digit>, accessed on March 3, 2024.
- [2] Altair HyperWorks CFD, “Boundary Conditions Types,” , 2024. URL [https://2021.help.altair.com/2021/hwdesktop/cfd/topics/acusolve/training\\_manual/boundary\\_condition\\_types\\_r.htm](https://2021.help.altair.com/2021/hwdesktop/cfd/topics/acusolve/training_manual/boundary_condition_types_r.htm), accessed on March 13, 2024.